An Augmented Lagrangian Method for Sparse SAR Imaging

H. Emre Güven, ASELSAN Inc., heguven@aselsan.com.tr, Turkey
Müjdat Çetin, SabancıUniversity, mcetin@sabanciuniv.edu, Turkey

Abstract

In this paper, we present a solution to the constrained ℓ_1-norm minimization problem for sparse SAR imaging. The techniques rely on the recent advances in the solution of optimization problems, based on the Augmented Lagrangian Methods (ALMs), namely the Alternating Direction Method of Multipliers. Here, we present an application of C-SALSA (an ALM for constrained optimization problems) to SAR imaging, and introduce a new weighting scheme to improve the sparsity of the reconstructions. We then compare the performances of several techniques to understand the effectiveness of the ALMs in the context of SAR imaging.

1 Introduction

In this paper we consider the problem of sparse reconstruction of SAR images using an Augmented Lagrangian approach to the optimization problem associated with the SAR observation model.

There are several sparsity-driven techniques in the context of SAR imaging [**?**, **?**], though an important factor hindering their use in practice is the excessively high computational cost of solving the associated optimization problem. From this standpoint, it is important to incorporate recent advances in optimization techniques, where the computational complexity associated with the solution of optimization problems has been receiving an increasing interest. The motivation for our work comes from our search for such computationally efficient algorithms for compressed sensing in SAR, with a potential for parallel implementation.

As such, Alternating Direction Method of Multipliers (ADMM) techniques have been successfully applied to signal and image recovery problems [**?**, 1]. provides a divide-and-conquer approach by splitting unconstrained multi-objective convex optimization problems, augmenting the Lagrangian of the convex optimization problem with a norm-squared error term, and using a non-linear block Gauss-Seidel approach on the resultant terms in the optimization problem. The resulting problem is guaranteed convergence under mild conditions [1].

In this work, we provide a framework for the application of the ADMM method C-SALSA (Constrained Split Augmented Lagrangian Shrinkage Algorithm) [1] to SAR imaging, and provide a refinement that enhances sparsity, inspired by the use of p-norms with $p < 1$ for feature-enhanced SAR imaging methods [2].

2 Background

2.1 SAR Observation Model

The SAR observation model can be considered linear in the relating the vector containing the SAR image pixels to the data vector, e.g., as in phase history data for spotlight mode SAR imaging. Mathematically speaking, we can denote the image vector to be constructed by sequentially indexed pixel-values $\mathbf{x} \in \mathbb{C}^N$ and the matrix $\mathbf{B} \in \mathbb{C}^{M \times N}$ relating $\mathbf{x}$ to the measurement vector $\mathbf{y} \in \mathbb{C}^{\mathbb{M}}$:

$$\mathbf{y} = \mathbf{B}\mathbf{x} + \mathbf{n}, \tag{1}$$

where $\mathbf{n} \in \mathbb{C}^M$ is the additive noise vector, typically from a normal distribution. The data $\mathbf{y}$ can lie in the phase history domain, in which case the matrix $\mathbf{B}$ would be a spatial Fourier transform type operator; or $\mathbf{y}$ can be a conventionally reconstructed image, in which case $\mathbf{B}$ would be a convolution operator representing the point spread function of the entire imaging process. In this paper, the data are assumed to be in the phase history domain, therefore a two-dimensional Fourier transform type model is appropriate for modeling the relation between the data vector and the unknown SAR image vector. In the reconstruction algorithms we use, however, the matrix is never formed explicitly but FFT's are performed to perform the associated matrix-vector products.

2.2 Sparse reconstruction approaches

In this paper, we consider and compare the use of feature-enhanced imaging method [2], focusing on the specific case of point-enhanced (PE) imaging where point-like features are preserved through the regularized form in (3), and C-SALSA [1] for the reconstruction of SAR images, as well as a modification of C-SALSA through the introduction of an iteratively updated diagonal weighting at the soft-thresholding step of the algorithm as described in the sequel. For the compressed sensing problem, where sparsity in the SAR images is in the spatial-domain, the problem can be cast as the minimization of the ℓ_1-norm of the SAR image vector;

$$\underset{\mathbf{x}}{\text{minimize}} \quad \|\mathbf{B}\mathbf{x} - \mathbf{y}\|_2^2 + \lambda \|\mathbf{x}\|_p \ . \tag{2}$$

with $p = 1$. Additionally, other sparse reconstruction techniques use p-norms with $p < 1$ with encouraging results [2].

An alternative form of the problem is such that the constraint comes from the error in the measurements, where the error norm is prescribed to be smaller than a radius ϵ suggested by the signal-to-noise ratio (SNR) that can be estimated from the data.

$$\begin{array}{ll} \underset{\mathbf{x}}{\text{minimize}} & \|\mathbf{x}\|_p \\ \text{subject to} & \|\mathbf{B}\mathbf{x}-\mathbf{y}\|_2 \leq \epsilon \end{array} \tag{3}$$

where the value of $p = 1$ is chosen to improve sparsity in the reconstructed images.

Motivated by the use of such norms, we propose to use an Augmented Lagrangian based algorithm for the reconstruction of SAR images, where a new weighting scheme is introduced. While it is possible to formulate an Augmented Lagrangian Method (ALM) directly for (2) with $p < 1$, we instead use the ADMM method C-SALSA [1], as well as a modification thereof using an iteratively reweighted soft-thresholding scheme based on the p-norm of the input to the soft-thresholding step at each iteration. Although an augmented Lagrangian method such as SALSA [4] for unconstrained convex optimization problems is in a more direct correspondence with the regularization based techniques such as in (3), we prefer the constrained form of the problem (2) with $p = 1$ due to its simplicity in its parameter choice where an estimate of the SNR can be obtained easily [1].

For the purposes of comparison, however, we first pick a regularization value λ to solve the problem (3) using the point-enhanced reconstruction algorithm [2], and in sequence, use the resulting value of the error norm to substitute for the value of ϵ in (2). In practice, a good selection of the error radius is given by $\epsilon = \sqrt{M^2 + 8M}\sigma$ [1] for a noise variance of σ^2, i.e., $E\left[\mathbf{n}\mathbf{n}^H\right] = \sigma^2\mathbf{I}$; while other choices of ϵ are certainly possible.

Further details regarding the Point-Enhanced Reconstruction Method (PERM) obtained by the imaging algorithm can be found in the references [2, **?**]. In the next section, we describe the algorithm C-SALSA [1], as well as the proposed modification obtained by the iteratively updated weighting therein.

3 ADMM applied to SAR Imaging

3.1 C-SALSA

The problem in (2) with $p = 1$ can be expressed in an unconstrained form as [1]:

$$\underset{\mathbf{x}}{\text{minimize}} \quad \|\mathbf{x}\|_1 + \iota_{E(\epsilon,\mathbf{I},\mathbf{y})}(\mathbf{B}\mathbf{x}) \tag{4}$$

where $\iota_{E(\epsilon,\mathbf{I},\mathbf{y})}(\mathbf{B}\mathbf{x})$ is the indicator function of the feasible set $E(\epsilon,\mathbf{I},\mathbf{y})$ such that

$$E(\epsilon,\mathbf{I},\mathbf{y}) = \left\{\mathbf{x}\in\mathbb{C}^N : \|\mathbf{B}\mathbf{x}-\mathbf{y}\|_2\right\} \leq \epsilon, \tag{5}$$

$$\iota_S(\mathbf{s}) = \begin{cases} 0, & \text{if } \mathbf{s}\in S \\ +\infty, & \text{if } \mathbf{s}\notin S \end{cases}. \tag{6}$$

Algorithm: ***C-SALSA*** [1]

1. Set $k = 0$, choose $\mu > 0$, $\mathbf{v}_0^{(1)}$, $\mathbf{v}_0^{(2)}$, $\mathbf{d}_0^{(1)}$, $\mathbf{d}_0^{(2)}$
2. **repeat**
3. $\mathbf{r}_k = \mathbf{v}_0^{(1)} + \mathbf{d}_0^{(1)} + \mathbf{B}^H\left(\mathbf{v}_0^{(2)} + \mathbf{d}_0^{(2)}\right)$
4. $\mathbf{u}_{k+1} = \left(\mathbf{I} + \mathbf{B}^H\mathbf{B}\right)^{-1}\mathbf{r}_k$
5. $\mathbf{v}_{k+1}^{(1)} = \mathbf{\Psi}_{\phi/\mu}\left(\mathbf{u}_{k+1} - \mathbf{d}_k^{(1)}\right)$
6. $\mathbf{v}_{k+1}^{(2)} = \mathbf{\Psi}_{\iota_{E(\epsilon,\mathbf{I},\mathbf{y})}}\left(\mathbf{B}\mathbf{u}_{k+1} - \mathbf{d}_k^{(2)}\right)$
7. $\mathbf{d}_{k+1}^{(1)} = \mathbf{d}_k^{(1)} - \mathbf{u}_{k+1} + \mathbf{v}_{k+1}^{(1)}$
8. $\mathbf{d}_{k+1}^{(2)} = \mathbf{d}_k^{(2)} - \mathbf{B}\mathbf{u}_{k+1} + \mathbf{v}_{k+1}^{(2)}$
9. $k \leftarrow k + 1$
10. **until** some stopping criterion is satisfied.

The vectors $\mathbf{v}_0^{(1)}$ and $\mathbf{d}_0^{(1)}$ are in $\mathbb{C}^N$, whereas $\mathbf{v}_0^{(2)}$ and $\mathbf{d}_0^{(2)}$ are in $\mathbb{C}^M$. The operators $\mathbf{\Psi}_{\phi/\mu}$ and $\mathbf{\Psi}_{\iota_{E(\epsilon,\mathbf{I},\mathbf{y})}}$ are the Moreau proximal maps for $\frac{1}{\mu}\phi(\mathbf{x}) = \frac{\|\mathbf{x}\|_1}{\mu}$ and $\iota_{E(\epsilon,\mathbf{I},\mathbf{y})}(s)$ given by

$$\mathbf{\Psi}_{\phi/\mu}(\mathbf{s}) = \text{soft}(\mathbf{y}, 1/\mu), \tag{7}$$

and

$$\mathbf{\Psi}_{\iota_{E(\epsilon,\mathbf{I},\mathbf{y})}}(\mathbf{s}) = \begin{cases} \mathbf{s}, & \text{if } \|\mathbf{s}-\mathbf{y}\|_2 \leq \epsilon \\ \mathbf{y} + \epsilon\frac{(\mathbf{s}-\mathbf{y})}{\|\mathbf{s}-\mathbf{y}\|_2}, & \text{if } \|\mathbf{s}-\mathbf{y}\|_2 > \epsilon \end{cases}, \tag{8}$$

respectively, where $\text{soft}(\mathbf{y}, 1/\tau)$ denotes the element-wise application of $y_i \rightarrow \text{sign}(y_i)\max\{|y_i| - \tau\}$ to entries y_i of $\mathbf{y}$ for $i = 1, \ldots, M$ [1].

For SAR imaging problem sizes that are relevant in practice, it is not desirable to form the matrix $\mathbf{B}$ due to prohibitively large dimensions. As such, the most critical in C-SALSA is its fourth step, where a matrix-vector equality is solved in each step of the iterative algorithm. Therefore, it is of utmost interest to perform this computation using fast transforms [1], such as the FFT.

Similar to medical imaging applications such as MRI and CT, SAR imaging can be viewed as an image recovery problem with partial Fourier domain observations, where the samples are available on a polar grid [5]. As a result, following an interpolation in the two-dimensional Fourier transform domain, it is possible to relate the resulting data vector to the SAR image through a 2-D FFT. Hence, the multiplications by $\mathbf{B}$ and $\mathbf{B}^H$ can be performed via 2-D FFT operations (that effectively perform the multiplication by a matrix $\mathbf{U}$ containing the Fourier basis vectors), and a masking operator (that effectively performs multiplication by a diagonal matrix $\mathbf{M}$ with only 1's and 0's along its diagonal, so that $\mathbf{M}\mathbf{M}^H = \mathbf{I}$) such that $\mathbf{B} = \mathbf{M}\mathbf{U}$. Such a matrix satisfies [1]:

$$\left(\mathbf{I} + \mathbf{B}^H\mathbf{B}\right)^{-1} = \mathbf{I} - \frac{1}{2}\mathbf{U}^H\mathbf{M}^H\mathbf{M}\mathbf{U} \tag{9}$$

and therefore step 4 of C-SALSA can be performed at the cost of $O(N\log N)$ multiplications [1]. In the examples in Section 4, (9) is implemented via 2-D FFT's and consequent masking in the Fourier domains as described above.

A commonly used stopping criterion is the relative difference of the iterates in comparison to the previous step [1, 2].

3.2 Iteratively Re-Weighted Augmented Lagrangian Method (IRWALM)

In this section, we provide a further refinement to C-SALSA, inspired by the effectiveness of p-norms used in the objective function with $p < 1$, as they improve sparsity compared to the case with $p = 1$. While the direct use of p-norms with $p < 1$ in (2) or (3) renders the problem non-convex, thus voiding any guarantees relating to global optimality of the solutions; a locally-optimal solution is provided nonetheless. A quasi-Newton method with a Hessian update scheme has been previously used successfully to obtain a solution to (3) in the SAR imaging context [2], which provides us the motivation to incorporate into the solution a weighting related to the p-norm of the solution for $p < 1$.

While it is possible to apply the ADMM techniques directly for the case with $p < 1$ for the constrained problem (2), in this paper we take a simpler approach where only the soft-thresholding step of the iterative algorithm is modified to incorporate a pre- and post-diagonal weighting related to the p-norm of the input to the associated soft-thresholding function.

Algorithm: IRWALM

1. Set $k = 0$, choose $\mu > 0$, $\mathbf{v}_0^{(1)}$, $\mathbf{v}_0^{(2)}$, $\mathbf{d}_0^{(1)}$, $\mathbf{d}_0^{(2)}$
2. **repeat**
3. $\mathbf{r}_k = \mathbf{v}_0^{(1)} + \mathbf{d}_0^{(1)} + \mathbf{B}^H \left(\mathbf{v}_0^{(2)} + \mathbf{d}_0^{(2)} \right)$
4. $\mathbf{u}_{k+1} = \left(\mathbf{I} + \mathbf{B}^H \mathbf{B} \right)^{-1} \mathbf{r}_k$
5. $\mathbf{W}_{k+1} = \text{diag} \left(|\mathbf{u}_{k+1} - \mathbf{d}_k^{(1)}|^{1-p} \right)$
6. $\mathbf{v}_{k+1}^{(1)} = \mathbf{W}_{k+1}^{-1} \left\{ \mathbf{\Psi}_{\phi/\mu} \left[\mathbf{W}_{k+1} \left(\mathbf{u}_{k+1} - \mathbf{d}_k^{(1)} \right) \right] \right\}$
7. $\mathbf{v}_{k+1}^{(2)} = \mathbf{\Psi}_{\iota_{E(\epsilon, \mathbf{I}, \mathbf{y})}} \left(\mathbf{B}\mathbf{u}_{k+1} - \mathbf{d}_k^{(2)} \right)$
8. $\mathbf{d}_{k+1}^{(1)} = \mathbf{d}_k^{(1)} - \mathbf{u}_{k+1} + \mathbf{v}_{k+1}^{(1)}$
9. $\mathbf{d}_{k+1}^{(2)} = \mathbf{d}_k^{(2)} - \mathbf{B}\mathbf{u}_{k+1} + \mathbf{v}_{k+1}^{(2)}$
10. $k \leftarrow k + 1$
11. **until** some stopping criterion is satisfied.

At each iteration, the wei gut s are updated based on the input to the soft-thresholding function. The weighting matrix is chosen to have diagonal entries proportional to the powers $(1 - p)$ of the absolute values of the elements in the input vector, i.e., $\mathbf{W} = \text{diag} \left(|\cdot|^{1-p} \right)$, where $(\cdot)$ is the input to the soft thresholding function. Thus, the soft-thresholding $\mathbf{\Psi}_{\phi/\mu}$ is replaced by $\mathbf{W}^{-1} \left\{ \mathbf{\Psi}_{\phi/\mu} \left[\mathbf{W}(\cdot) \right] \right\}$, which provides the basis for improved sparsity by incorporating the effect of p-norm with $p < 1$ with a slight modification of the Augmented Lagrangian Method for $p = 1$.

4 Results

For the examples, we form the phase history data from reference SAR images obtained from wide-angle, high bandwidth SAR returns using the method described in [3]. L denotes the bandwidth reduction ratio in each dimension (in terms of the bandwidth used to reconstruct the reference image.) The number of available data samples is $M = L^2 N$, where N is the number of phase history samples in the full-bandwidth data used to form the reference image.

Table 1 shows the results obtained with the methods PERM and C-SALSA for the case with $p = 1$; whereas Table 2 shows the results for $p = 0.5$. The first two columns on Tables 1 and 2 are the times it took to compute the results in Matlab with PERM and IRWALM, respectively. Timing results are based on our implementation (non-optimized MATLAB code) run on a Macbook Pro with an Intel Core i7 processor with 6 GB RAM. The signal to noise ratio in the observations was 30 dB, and the iterations in each casae were stopped when the relative difference between successive iterations dropped below 0.005. The third and fourth columns in Tables 1 and 2 are the ratios of the data fidelity errors (data fidelity error in the reconstruction via C-SALSA and IRWALM divided by the data fidelity error in the reconstruction via PERM), as well as the 1-norms of the reconstructions. For similar data fidelity errors with PERM and IRWALM, the 1-norms of the reconstructions are slightly less for IRWALM, while the computation time is significantly reduced (4.8–5.8 times for $p = 1$ and 6.3–10 times for $p = 0.5$, respectively.)

Data	t_{pe}	t_{irwalm}	$\frac{\varepsilon}{\varepsilon_{pe}}$	$\frac{\|x\|_1}{\|x_{pe}\|_1}$
Slicy ($L = 2/8$)	1.8 s	0.5 s	0.9845	0.73
Backhoe ($L = 3/8$)	8.7 s	1.2 s	0.9995	0.97
Backhoe ($L = 2/8$)	8.4 s	1.3 s	0.9984	0.95
Backhoe ($L = 1/8$)	7.2 s	1.5 s	0.9987	0.92

Table 1: Computation times, error- and ℓ_1-norm-ratios for PERM and C-SALSA ($p = 1$).

Data	t_{pe}	t_{irwalm}	$\frac{\varepsilon}{\varepsilon_{pe}}$	$\frac{\|x\|_1}{\|x_{pe}\|_1}$
Slicy ($L = 2/8$)	2.0 s	0.5 s	0.9449	0.90
Backhoe ($L = 3/8$)	32.1 s	3.2 s	0.9993	0.89
Backhoe ($L = 2/8$)	32.0 s	4.0 s	0.9969	0.88
Backhoe ($L = 1/8$)	30.3 s	4.8 s	0.9960	0.84

Table 2: Computation times, error- and ℓ_1-norm-ratios for PERM and IRWALM ($p = 0.5$).

Figure 1 shows the reconstruction the results for Slicy with $L = 2/8$; while **Figures 2, 3, 4** show the Backhoe results for $L = 3/8$, $L = 2/8$, and $L = 1/8$, respectively. Visually similar results are obtained in general by PERM and C-SALSA (for the case with $p = 1$), while sparsity of reconstructions is improved by the use of $p = 0.5$ in comparison with both approaches.

5 Conclusions

In this paper, we investigate the use of Augmented Lagrangians in the context of sparse SAR image reconstruction from undersampled measurements. We propose a new iteratively reweighted algorithm that enhances sparsity in the reconstructed images. The results show that it is possible to obtain faster solutions than comparable solutions for desirable levels of accuracy. The future work will focus on more detailed analyses of the solutions via ALMs, as well as parallel / fast implementations for practical use.

References

[1] M. Figueiredo et al: *C-SALSA*

[2] M. Cetin et al: *IEEE Trans. Image Processing*, 2001.

[3] R. L. Moses, L. Potter, and M. Çetin: *Wide Angle SAR Imaging*, SPIE Defense and Security Symposium, Algorithms for Synthetic Aperture Radar Imagery XI, Eds., E. G. Zelnio and F. D. Garber, Orlando, Florida, April 2004.

[4] M. Figueiredo et al: *SALSA*

[5] C. V. Jakowatz, Jr., D. E. Wahl, P. H. Eichel, D. C. Ghiglia, and P. A. Thompson: *Spotlight-Mode Synthetic Aperture Radar: A Signal Processing Approach*, Norwood, MA: Kluwer, 1996.

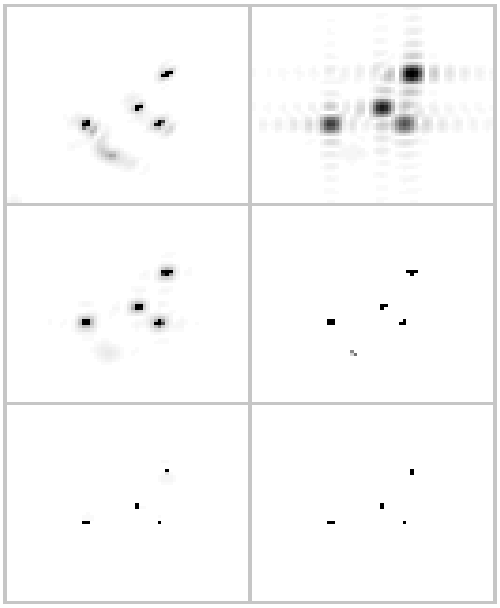

Figure 1: Slicy, $L = 2/8$. (upper-left) reference image, (upper-right) conventional reconstruction, (mid-left) PERM with $p = 1$, (mid-right) C-SALSA,(lower-left) PERM $p = 0.5$, (lower-right) IRWALM $p = 0.5$

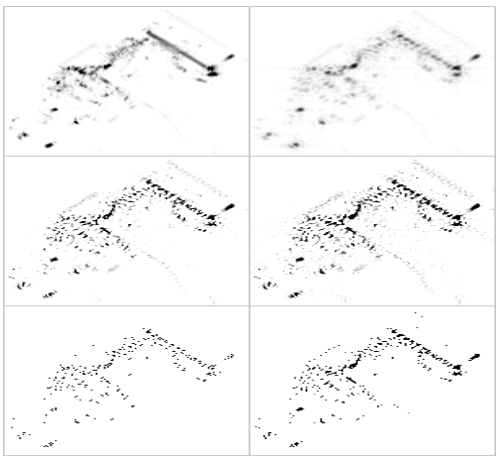

Figure 2: Backhoe, $L = 3/8$. (upper-left) reference image, (upper-right) conventional reconstruction, (mid-left) PERM with $p = 1$, (mid-right) C-SALSA, (lower-left) PERM $p = 0.5$, (lower-right) IRWALM $p = 0.5$

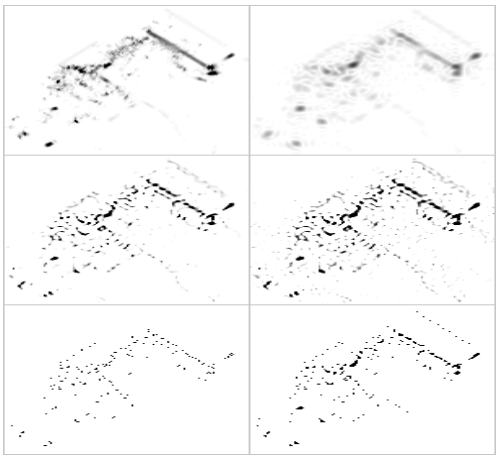

Figure 3: Backhoe, $L = 2/8$. (upper-left) reference image, (upper-right) conventional reconstruction, (mid-left) PERM with $p = 1$, (mid-right) C-SALSA, (lower-left) PERM $p = 0.5$, (lower-right) IRWALM $p = 0.5$

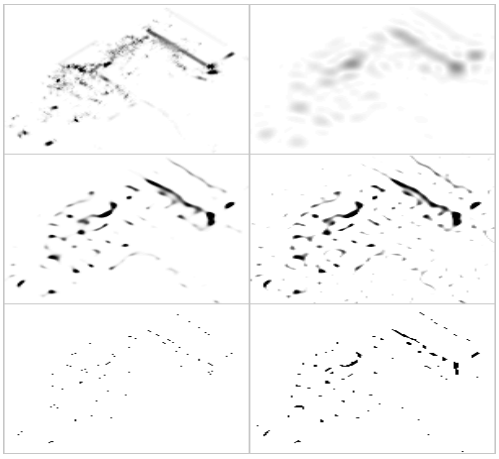

Figure 4: Backhoe, $L = 1/8$. (upper-left) reference image, (upper-right) conventional reconstruction, (mid-left) PERM with $p = 1$, (mid-right) C-SALSA, (lower-left) PERM $p = 0.5$, (lower-right) IRWALM $p = 0.5$